Inorganic Chemistry
Article

Inorg. Chem. **2010**, *49*, 5957–5962 **5957**
DOI: 10.1021/ic100452m

Synthesis and Thermal Stability of the Solid Solution AFeO$_2$ (A = Ba, Sr, Ca)

Takafumi Yamamoto,[†,‡] Zhaofei Li,[§] Cédric Tassel,[†,‡] Naoaki Hayashi,[∥] Mikio Takano,[§] Masahiko Isobe,[⊥] Yutaka Ueda,[⊥] Kenji Ohoyama,[⊗] Kazuyoshi Yoshimura,[‡] Yoji Kobayashi,[†] and Hiroshi Kageyama*[,†,‡,§]

[†]*Department of Energy and Hydrocarbon Chemistry, Graduate School of Engineering, Kyoto University, Kyoto 615-8510, Japan,* [‡]*Department of Chemistry, Graduate School of Science, Kyoto University, Kyoto 606-8502, Japan,,* [§]*Institute for Integrated Cell-Material Sciences, and* [∥]*Graduate School of Human and Environmental Studies, Kyoto University, Kyoto 606-8501, Japan,* [⊥]*Institute for Solid State Physics, University of Tokyo, 5-1-5 Kashiwanoha, Kashiwa, Chiba 277-8581, Japan, and* [⊗]*Institute for Materials Research, Tohoku University, 2-1-1 Katahira, Aoba-ku, Sendai 980-8577, Japan*

Received March 8, 2010

We have studied the A-site substitution effect on the structural, thermal, and magnetic properties of the infinite layer iron oxide AFeO$_2$ (A = alkali-earth elements) with an FeO$_4$ square-planar coordination. Together with the previous study showing a total substitution by Ca, Ba substitution is found to be tolerable up to 30%, presenting almost the same substitutional range as that found in ACuO$_2$ under high pressure. Notably, Ba substitution shows little influence on the magnetic properties, in contrast to expectations from first principles calculations. The temperature at which oxidation to an AFeO$_{2.5}$ phase occurs and its transformation rate show a wide variation tunable solely by the out-of-plane distance.

1. Introduction

Topochemical reactions such as ion exchange and intercalation reactions provide unique access to metastable crystalline oxide solids, novel structures, and local coordination that can not be obtained by conventional high temperature solid state reactions. Examples include H[Ca$_2$Na$_{n-3}$Nb$_n$O$_{3n+1}$] ($3 \le n \le 7$),[1] (CuX)LaNb$_2$O$_7$ (X = Cl, Br),[2] H$_{1.8}$[Bi$_{0.21}$Sr$_{0.80}$-Na$_{0.95}$Nb$_3$O$_{10}$],[3] which were prepared, respectively, from layered perovskites K[Ca$_2$Na$_{n-3}$Nb$_n$O$_{3n+1}$], RbLaNb$_2$O$_7$, and Bi$_{1.8}$Sr$_{0.2}$O$_2$[Bi$_{0.2}$Sr$_{0.8}$NaNb$_3$O$_{10}$]. However, the reaction processes and driving forces that allow the modification of structures and composition at low temperature are still far from being satisfactorily understood. This is in contrast to the well-known reaction mechanisms in synthetic organic chemistry. However, this is crucial for further developing topochemical routes and would ultimately help to lower working temperatures of solid oxide fuel cells and oxygen membranes.

An unprecedented FeO$_4$ square planar coordination has been recently realized in SrFeO$_2$ by reducing perovskite SrFeO$_3$ (Figure 1a) with CaH$_2$ at low temperatures.[4] As seen in Figure 1c, the structure of SrFeO$_2$ is made up of corner-shared FeO$_4$ square planes in between strontium atoms and is isostructural with the infinite layer (IL) structure SrCuO$_2$.[5,6] Surprisingly, first-principles calculations revealed that this new material is a thermodynamically stable phase.[7,8] From the isomer shift of Mössbauer spectra, we found that the Fe^{2+} in SrFeO$_2$ is indeed more strongly bonded to neighboring O^{2-} than those of any other existing divalent ferrous compounds. This utmost feature allows this material to achieve a magnetic order well above room temperature (T_N = 473 K)[4] and explains why a spin-state transition is realized for the first time in a four-coordinated metal center.[9,10] This feature also preserves the square planes during structural changes, even if some distortion occurs. SrFeO$_2$ is susceptible to substantial positive chemical pressure; the substitution of the strontium site with calcium, having a smaller ionic radius, is possible up to as much as 80%. A further and complete substitution to CaFeO$_2$ results in a considerable distortion of the FeO$_4$

*To whom correspondence should be addressed. E-mail: kage@scl.kyoto-u.ac.jp.

(1) Jacobson, A. J.; Johnson, J. W.; Lewandowski, J. T. *Inorg. Chem. Soc.* **1985**, *24*, 3727–3729.
(2) Kodenkandath, T. A.; Lalena, J. N.; Zhou, W. L.; Carpenter, E. E.; Sangregorio, C.; Falster, A. U.; Simmons, W. B., Jr.; O'Connor, C. J.; Wiley, J. B. *J. Am. Chem. Soc.* **1999**, *121*, 10743–10746.
(3) Sugimoto, W.; Shirata, M.; Sugahara, Y.; Kuroda, K. *J. Am. Chem. Soc.* **1999**, *121*, 11601–11602.
(4) Tsujimoto, Y.; Tassel, C.; Hayashi, N.; Watanabe, T.; Kageyama, H.; Yoshimura, K.; Takano, M.; Ceretti, M.; Ritter, C.; Paulus, W. *Nature* **2007**, *450*, 1062–1065.
(5) Siegrist, T.; Zahurak, S. M.; Murphy, D. W.; Roth, R. S. *Nature* **1988**, *334*, 231–232.
(6) Takano, M.; Takeda, Y.; Okada, H.; Miyamoto, M.; Kusaka, T. *Physica C* **1989**, *159*, 375–378.
(7) Xiang, H. J.; Wei, S. H.; Whangbo, M. H. *Phys. Rev. Lett.* **2008**, *100*, 167207.
(8) Pruneda, J. M.; Iñiguez, J.; Canadell, E.; Kageyama, H.; Takano, M. *Phys. Rev. B* **2008**, *78*, 115101.
(9) Kawakami, T.; Tsujimoto, Y.; Kageyama, H.; Chen, X.; Tassel, C.; Fu, L.; Kitada, A.; Saito, S.; Sekiya, Y.; Makino, Y.; Okada, T.; Yagi, T.; Hayashi, N.; Yoshimura, K.; Nasu, S.; Podloucky, R.; Takano, M. *Nat. Chem.* **2009**, *1*, 371–376.
(10) Whangbo, M. H.; Köhler, J. *Nat. Chem.* **2009**, *1*, 351–352.

Published on Web 05/28/2010

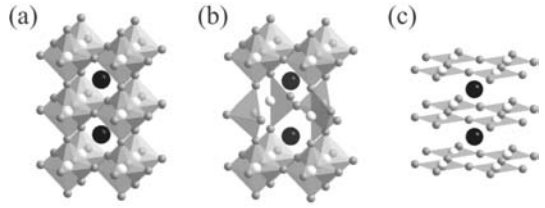

Figure 1. Schematic representation of the structures of perovskite $SrFeO_3$ (a), brownmillerite $SrFeO_{2.5}$ (b), infinite layer $SrFeO_2$ (c). Black, white, and gray spheres represent Sr, Fe, and O atoms, respectively.

square plane toward a tetrahedron.[11,12] The conversion from $SrFeO_3$ to $SrFeO_2$ (or vice versa) proceeds via the brownmillerite-type intermediate $SrFeO_{2.5}$ (Figure 1b) at temperatures as low as 400 K,[13] thereby involving not only extraction (insertion) of oxide ions but also drastic rearrangement of the oxide ions in the basal framework.

In this paper, we report on the effect of negative chemical pressure on the structural and magnetic properties by the Sr-to-Ba substitution. Unlike the case of positive chemical pressure, the IL structure $(Sr_{1-y}Ba_y)FeO_2$ is found to exist only up to 30%. The substitutional and thermal stabilities as well as magnetic properties of this Ba-substituted and the Ca-substituted systems are discussed.

2. Experimental Section

First, we prepared oxygen deficit perovskite oxides $(Sr_{1-y}Ba_y)FeO_{3-\delta}$ ($0 < \delta < 0.5$) for $y = 0.1$, 0.2, 0.3, and 0.4. Mixtures of stoichiometric amount of $SrCO_3$ (99.99%), $BaCO_3$ (99.99%), and Fe_2O_3 (99.99%) were weighed, ground, pelletized, and heated at 1473 K for 2 days in air with one intermediate grinding. Subsequently, the precursors of about 0.25 g were finely ground with two-molar excess of CaH_2 in an Ar-filled glovebox, sealed in an evacuated Pyrex tube (volume 15 cm^3) with a residual pressure less than 1.3×10^{-8} MPa, and reacted at 553 K for 3 days. The residual CaH_2 and the byproduct CaO were removed by washing out with NH_4Cl/methanol solution (0.15 mol/L). For the study of low-temperature powder X-ray diffraction (XRD) and thermogravimetry (TG), $(Sr_{1-x}Ca_x)FeO_2$ ($x = 0.0$, 0.2, 0.4, 0.6, 0.8) were synthesized according to the procedure as described previously.[11]

The sample purity was checked by XRD profile using a Mac Science M18XHF diffractometer equipped with a graphite monochromator and a CuK_α radiation ($\lambda = 1.54056$ Å). Low-temperature XRD data of $(Sr_{1-x}Ca_x)FeO_2$ and $(Sr_{1-y}Ba_y)FeO_2$ for $x = 0.0$, 0.4, 0.8 and $y = 0.3$ were collected for 10−290 K on a Mac Science MXP18 diffractometer equipped with a closed-cycle He refrigerator installed at the Institute for Solid State Physics, University of Tokyo. A monochromatized CuK_α source was used and each scan was performed on a 2θ range of 20−70° with an angular step of 0.02° and a counting time of 2.5°/sec. The peak positions were calibrated against Si as an internal standard, and the lattice parameters were obtained with a least-squares method.

High-resolution synchrotron XRD experiments on $(Sr_{1-y}Ba_y)FeO_2$ ($y = 0.1$, 0.2, 0.3) were performed at room temperature using a large Debye−Scherrer camera installed at the Japan Synchrotron Radiation Research Institute SPring-8 BL02B2. We used an imaging plate as a detector. Incident beams from a bending magnet were monochromatized to 0.42026 Å. The finely ground powder samples were filtered by a strainer with 32-μm-square holes and put into a Pyrex capillary of inner 0.1 mm diameter. The capillary was rotated during measurements to reduce preferential orientation. The obtained synchrotron XRD data were analyzed by the Rietveld method by using RIETAN-2000 program.[14] The agreement indices used were *R*-weighted pattern, $R_{wp} = [\sum w_i(y_{io} - y_{ic})^2/\sum w_i(y_{io})^2]^{1/2}$, *R*-pattern, $R_p = \sum|y_{io} - y_{ic}|/\sum(y_{io})$, and goodness of fit (GOF), $\chi^2 = [R_{wp}/R_{exp}]^2$, where $R_{exp} = [(N - P)/\sum w_i y_{io}^2]^{1/2}$, y_{io} and y_{ic} are the observed and calculated intensities, w_i is the weighting factor, *N* is the total number of y_{io} data when the background is refined, and *P* is the number of adjusted parameters.

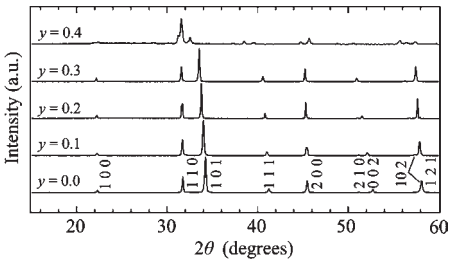

Figure 2. Powder XRD patterns of $(Sr_{1-y}Ba_y)FeO_2$. All the patterns except $y = 0.4$ could be indexed on the basis of the tetragonal IL structure. The $y = 0.4$ sample is identified as $(Sr_{0.6}Ba_{0.4})FeO_{2.5}$.

Powder neutron diffraction (ND) experiment on $(Sr_{0.8}Ba_{0.2})FeO_2$ ($y = 0.2$) at room temperature was carried out on the Kinken powder diffractometer with multicounters for High Efficiency and high Resolution MEasurementS, HERMES, of the Institute for Materials Research, Tohoku University, installed at a guide hall of the JRR-3 reactor in the Japan Atomic Energy Agency (JAEA), Tokai.[15] The incident neutron with a wavelength of 1.82646 Å was monochromatized by the 331 reflection of a vent Ge crystal. A 12′-blank-sample18′ collimation was employed. A polycrystalline sample of 3 g mass was placed into a vanadium cylinder. The data were collected with a step-scan procedure using 150 neutron detectors in a 2θ range from 3° to 153° with a step width of 0.1°.

Thermogravimetric data of $(Sr_{1-x}Ca_x)FeO_2$ ($x = 0.0$, 0.2, 0.4, 0.6, 0.8) and $(Sr_{1-y}Ba_y)FeO_2$ ($y = 0.2$) were collected using Rigaku Thermo plus (TG 8120). The sample of around 15 mg was put in a Pt pan, and α-Al_2O_3 was used as a reference material. The measurements were performed while heating the sample at 10 K min^{-1}. The samples after being heated were identified by in-house XRD measurements.

Mössbauer spectra on $(Sr_{1-y}Ba_y)FeO_2$ for $y = 0.1$, 0.2, and 0.3 were taken at room temperature in transmission geometry by using a ^{57}Co/Rh γ-ray source. The source velocity was calibrated by α-Fe as a reference material.

3. Results and Discussions

3.1. Crystal Structure. Figure 2 shows the XRD patterns of samples obtained by hydride reduction from the precursor $(Sr_{1-y}Ba_y)FeO_{3-\delta}$ ($0 < \delta < 0.5$) for $y = 0$−0.4. The XRD profiles for $0 \le y \le 0.3$ are very similar to each other and are readily indexed on the basis of the tetragonal unit cell without any peaks associated with impurities or super-reflections. However, the profile for $y = 0.4$ is assigned as $(Sr_{0.6}Ba_{0.4})FeO_{2.5}$ with the $Ba_2Fe_2O_5$-type structure.[16] The lattice parameters $a = 6.829(1)$ Å,

(11) Tassel, C.; Watanabe, T.; Tsujimoto, Y.; Kitada, A.; Sumida, Y.; Yamamoto, T.; Kageyama, H.; Hayashi, N.; Takano, M.; Yoshimura, K. *J. Am. Chem. Soc.* **2008**, *130*, 3764–3765.
(12) Tassel, C.; Pruneda, J. M.; Hayashi, N.; Watanabe, T.; Kitada, A.; Tsujimoto, Y.; Kageyama, H.; Yoshimura, K.; Takano, M.; Nishi, M.; Oyama, K.; Mizumaki, M.; Kawamura, N.; Íñiguez, J.; Canadell, E. *J. Am. Chem. Soc.* **2008**, *131*, 221–229.
(13) Hayward, M. A.; Rosseibsky, M. J. *Nature* **2007**, *450*, 960–961.
(14) Izumi, F.; Ikeda, T. *Mater. Sci. Forum* **2000**, *321−324*, 198–203.
(15) Ohoyama, K.; Kanouchi, T.; Nemoto, M.; Kajitani, T.; Yamauchi, Y. *Jpn. J. Appl. Phys.* **1998**, *37*, 3319–3326.

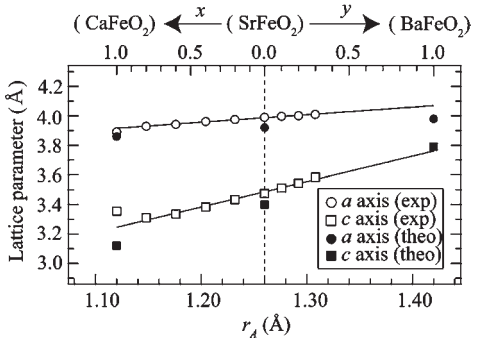

Figure 3. Lattice parameters of $(Sr_{1-x}Ca_x)FeO_2$[11,12] and $(Sr_{1-y}Ba_y)$-FeO_2 (this study). Open symbols represent the experimental values, while closed symbols represent the theoretical ones.[7] The error bars are within the size of the symbols. Solid lines were obtained by a least-squares fit. The deviation from the linear relation for $CaFeO_2$ is due to the distorted IL structure.[12].

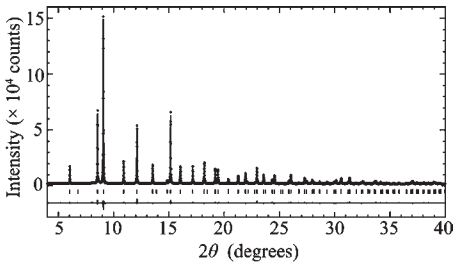

Figure 4. Structural characterization of $Sr_{0.7}Ba_{0.3}FeO_2$ ($y = 0.3$) by the Rietveld refinement of synchrotron XRD data at room temperature. The overlying crosses and the solid line represent the observed and the calculated intensities. The bottom solid line represents the difference between the observed intensity and the calculated intensity. The ticks correspond to the position of the calculated Bragg peaks of $(Sr_{0.7}Ba_{0.3})FeO_2$.

$b = 11.454(1)$ Å, $c = 23.11(4)$ Å and $\beta = 99.261(8)°$ are reasonable considering those of $BaFeO_{2.5}$ ($a = 6.969$ Å, $b = 11.724$ Å, $c = 23.408$ Å, $\beta = 98.372°$).[16] We could not obtain the IL $(Sr_{0.6}Ba_{0.4})FeO_2$ phase even with modified reaction temperature and time. The lattice parameters of the IL phase including the Ca substituted case are depicted in Figure 3 as a function of the average radius of the *A*-site cation, r_A, derived by assuming $r_{Ca} = 1.12$ Å, $r_{Sr} = 1.26$ Å, and $r_{Ba} = 1.42$ Å.[17] For comparison, theoretical lattice parameters of $CaFeO_2$, $SrFeO_2$, and $BaFeO_2$ obtained by first-principles calculations[7,8] are presented. The linear increase of the lattice parameters with r_A suggests the successful formation of the IL structure. The lines obtained by the least-squares fit of the experimental data are located slightly higher than theoretically predicted values except the *c* axis of the hypothetical IL phase $BaFeO_2$.

The synchrotron XRD data for the Ba-substituted samples ($y = 0.1$, 0.2, 0.3) also show a simple tetragonal unit cell. Absence of any broadening, splitting of peaks, and super-reflections as found in $CaFeO_2$[12] suggests formation of a well-crystallized and non-distorted IL structure. Accordingly, we performed Rietveld structural refinements for the synchrotron XRD data assuming, as an initial model, the ideal IL structure belonging to the *P*4/*mmm* space group with Sr/Ba on 1*d* (0.5, 0.5, 0.5), Fe on 1*a* (0, 0, 0), and O on 2*f* (0.5, 0, 0), where Ba and Sr atoms were set to be statistically disordered. All the refinements led to good fits, providing reasonable reliability factors $R_{wp} = 2.41\%$, $\chi^2 = 2.38$ for $y = 0.1$, $R_{wp} = 3.21\%$, $\chi^2 = 3.80$ for $y = 0.2$, and $R_{wp} = 3.16\%$, $\chi^2 = 3.18$ for $y = 0.3$ (see Figure 4, Figures 1S and 2S, and Table 1). Reasonably small atomic displacement parameters (*B*) for each refinement indicate that the Ba/Sr, Fe, and O atoms are positioned at the assumed sites.

To get more precise information on the oxygen position and its site occupation, we performed Rietveld refinement for the powder ND data of $(Sr_{0.8}Ba_{0.2})FeO_2$. The ND profile at room temperature included magnetic Bragg reflections, which were taken into account for the refinement, as will be discussed in detail later. The fit once again led to a reasonably small displacement parameter ($B = 1.12(8)$) for oxygen atoms (and other atoms) and $R_{wp} = 7.41\%$, $\chi^2 = 2.20$, as shown in Figure 5 and Table 1. When allowed to change, the oxygen occupancy factor was refined approximately to unity within error (1.005 (11)), indicating no oxygen deficiency. All these results together with the previous ones[11,12] led us to conclude that the ideal IL structure can tolerate up to 30% of the Ba-substitution and up to 80% of the Ca-substitution, namely, with r_A ranging from 1.15 to 1.31 Å. It is surprising that the solubility range of the IL structure is nearly the same as the cupric oxides $ACuO_2$ ($0 \le x < 0.9$, $0 \le y \le 0.33$) obtained by high temperature and high pressure synthesis.[6]

The bond valence sum (BVS) calculations[18] based on the synchrotron XRD data gave (*A*, Fe) = (+1.95, +1.95) for $y = 0.1$, (+1.99, +1.95) for $y = 0.2$ and (+2.00, +1.93) for $y = 0.3$. As shown in Figure 6, the BVS plotted as a function of r_A follows a linear relation for both *A* and Fe and hence validates once again the formation of the solid solution. Here, we would like to point out that while the Ca-substituted IL structure tolerates large deviation of the bond valences from the formal value (i.e., (*A*, Fe) = (+1.71, +2.15) for $x = 0.8$),[11] the Ba-substituted IL structure is only accessible up to $y \sim 0.3$ with (*A*, Fe) = (+2.00, +1.93). This should be related to the difficulty of Fe to take an unstable valence state of +1. Since the BVS of Fe is determined almost exclusively by the Fe−O distance within the FeO_2 layer, the in-plane length is likely to determine the solubility range of the IL structure. Note, however, that the IL cuprates $ACuO_2$ show a different variation of BVS, (*A*, Cu) = (+1.94, +2.06) ∼ (+2.41, +1.85), suggesting a different stabilization factor.

3.2. Magnetic Properties. The room-temperature ^{57}Fe Mössbauer spectra of $(Sr_{1-y}Ba_y)FeO_2$ for $y = 0.1$, 0.2, and 0.3, shown in Figure 7, Figures 3S and 4S consist of a single magnetically split sextet together with a small paramagnetic doublet peak. The obtained spectra were fitted by a Lorentzian function, and the results are summarized in Table 2. The doublet in each spectrum arises from a trivalent-iron-containing paramagnetic amorphous impurity formed by decomposition and over-reduction of the precursor $AFeO_{2.5}$ phase to Fe(0) that was then oxidized to Fe(III) upon exposure to air. Such an impurity

(16) Zou, X. D.; Hovmöller, S.; Parras, M.; Gonzalez-Calbet, J. M.; Vallet-Regi, M.; Grenier, J. C. *Acta Crystallogr.* **1993**, *A49*, 27–35.
(17) Shannon, R. D. *Acta Crystallogr.* **1976**, *A32*, 751–767.
(18) Brown, I. D.; Altermatt, D. *Acta Crystallogr.* **1985**, *B41*, 244–247.

Table 1. Rietveld Refinement for $(Sr_{1-y}Ba_y)FeO_2$ (y = 0.1, 0.2, 0.3)[a]

		y in $(Sr_{1-y}Ba_y)FeO_2$			
site		0.1 (SXRD)	0.2 (SXRD)	0.2 (ND)	0.3 (SXRD)
a (Å)		3.99794(3)	4.00059(3)	4.0014(1)	4.00896(4)
c (Å)		3.51198(3)	3.54538(4)	3.5457(2)	3.58441(5)
B in Sr/Ba (Å^2)	1d (0.5, 0.5, 0.5)	0.428(8)	0.49(1)	0.76(7)	0.50(1)
B in Fe (Å^2)	1a (0, 0, 0)	0.42(1)	0.49(2)	0.54(9)	0.51(2)
B in O (Å^2)	2f (0.5, 0, 0)	0.58(4)	0.64(5)	1.12(8)	0.74(5)
A−O (Å)		2.6607	2.6728	2.6732	2.6889
Fe−O (Å)		1.9990	2.0003	2.0007	2.0045
moment (μ_B)				3.3	
R_{wp} (%)		2.42%	3.21%	7.41%	3.16%
R_p (%)		1.55%	2.08%	5.65%	2.15%
χ^2		2.36	3.80	2.20	3.18

[a] SXRD and ND represent synchrotron X-ray diffraction and neutron diffraction. All the refinements were performed by using the ideal IL structure, $P4/mmm$ space group with A = $(Sr_{1-y}Ba_y)$ on 1d, Fe on 1 and O on 2f.

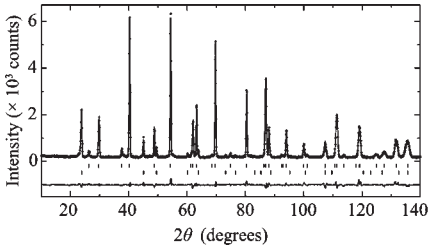

Figure 5. Structural characterization of $Sr_{0.2}Ba_{0.8}FeO_2$ (y = 0.2) by the Rietveld refinement of ND data at room temperature. The upper and lower ticks correspond to the position of the calculated chemical and magnetic Bragg peaks of $(Sr_{0.8}Ba_{0.2})FeO_2$.

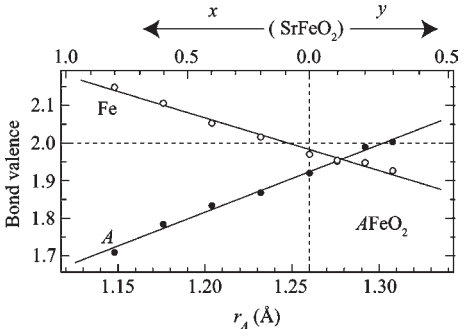

Figure 6. Bond valence sum for A (closed) and Fe (open) in $(Sr_{1-x}Ca_x)FeO_2$ or $(Sr_{1-y}Ba_y)FeO_2$. Here we assumed $r_o(A)$ = $(1 - y)$ $r_o(Sr)$ + y $r_o(Ba)$ where $r_o(Fe)$ = 1.734 Å, $r_o(Ba)$ = 2.285 Å, $r_o(Sr)$ = 2.118 Å.[18] Solid lines were obtained by a least-squares fit. Values for $(Sr_{1-x}Ca_x)FeO_2$ were taken from the previous study.[11]

phase was also observed upon the synthesis of $(Sr_{1-x}Ca_x)FeO_2$.[12] The values of isomer shift (*IS*) and quadrupole splitting (*QS*) for the sextet are very close to those of $SrFeO_2$ and the full width at half-maximum (fwhm) is resolution limited, further supporting the structural analysis of the present compounds based on the ideal IL structure. The Ba-concentration dependence of the hyperfine field (*HF*) shows that the iron ion stays in a divalent high-spin (S = 2) state and that the Néel temperature T_N decreases only slightly with Ba-concentration. The same tendency is seen for $(Sr_{1-x}Ca_x)FeO_2$ ($x \leq 0.8$).[12] Since the difference between S_1 and S_2 in Figure 7 is close to that of $SrFeO_2$ and to the value of QS above T_N in $SrFeO_2$, the magnetic moments in the magnetically ordered state are considered to align perpendicularly to the c axis, as in the case of $SrFeO_2$.

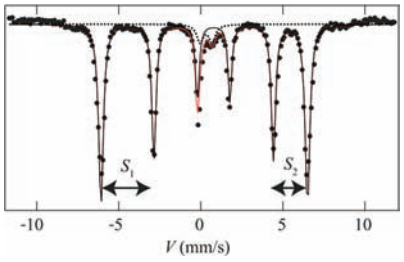

Figure 7. Mössbauer spectrum for $(Sr_{0.7}Ba_{0.3})FeO_2$ at room temperature. Circles denote the experimental data. A black solid line is the spectrum for $(Sr_{0.7}Ba_{0.3})FeO_2$ and a broken line is that from an over-reduced, decomposed impurity formed during the hydride reaction. A red line represents a total fit. S_1 and S_2 are the relative shifts of the peaks.

As mentioned above, the magnetic order for $(Sr_{0.8}Ba_{0.2})FeO_2$ at ambient temperature was also probed by the ND data. Well-developed magnetic reflections characterized as $((2h + 1)/2, (2k + 1)/2, (2l + 1)/2)$, where h, k, and l are integers, indicate the (π, π, π) type spin-structure. The Rietveld analysis demonstrated that the magnetic moments are 3.3 μ_B per iron and align in the ab plane in agreement with the Mössbauer results. A slight decrease of T_N with y is expected from the *HF* change. A linear extrapolation of the *HF* versus y curve to $y \rightarrow 1$ yielded the *HF* of 36 T for the hypothetical phase $BaFeO_2$. This value is very close to *HF* = 35 T obtained for the distorted IL $CaFeO_2$ at room temperature.[12] It follows that $BaFeO_2$ would have a similar T_N as $CaFeO_2$ (T_N = 433 K), at most 40 K lower than that of $SrFeO_2$.

A decrease in T_N in the Ba-substituted IL compound has been anticipated from the theoretical studies by Xiang et al.[7] They showed that the dominating spin exchange paths of $SrFeO_2$ are J_1 = 8.68 meV and J_2 = 2.23 meV, where J_1 is the intralayer Fe−O−Fe superexchange and J_2 is the interlayer Fe−Fe exchange coupling constants.[7] They also considered the hypothetical phase $BaFeO_2$ and obtained J_1 = 5.81 meV and J_2 = 1.34 meV. In the framework of the mean-field theory and the Monte Carlo simulation, it can be assumed that the T_N scales linearly with J_1 so long as the J_1/J_2 ratio remains constant.[19] Then, the T_N of $BaFeO_2$ is estimated as $473 \times (5.81/8.68) = 303$ K, which is, however, much lower than that estimated from the experimental data. The reason for the significant deviation

(19) Whangbo, M., private communication.

Table 2. Fitting Parameters of Mössbauer Spectra for $(Sr_{1-y}Ba_y)FeO_2$ (y = 0.1, 0.2, 0.3)[a]

y	*IS* (mm/s)	*HF* (T)	*QS* (mm/s)	fwhm (mm/s)	area (%)
0.0 [4]	0.498	40.1	1.16	0.28	100
0.1	0.493 (0.321)	39.6 (0.0)	1.15 (0.74)	0.31 (0.47)	91 (9)
0.2	0.495 (0.321)	39.1 (0.0)	1.14 (0.72)	0.31 (0.47)	95 (5)
0.3	0.497 (0.322)	39.0 (0.0)	1.15 (0.74)	0.31 (0.47)	94 (6)

[a] *IS*, *HF*, *QS*, fwhm, and area represent isomer shift, hyperfine field, quadrupole splitting, full width at half-maximum, and area percentage of total fit, respectively. We used the values of $SrFeO_2$ in previous study.[4] The values in parentheses are from the paramagnetic amorphous impurity.

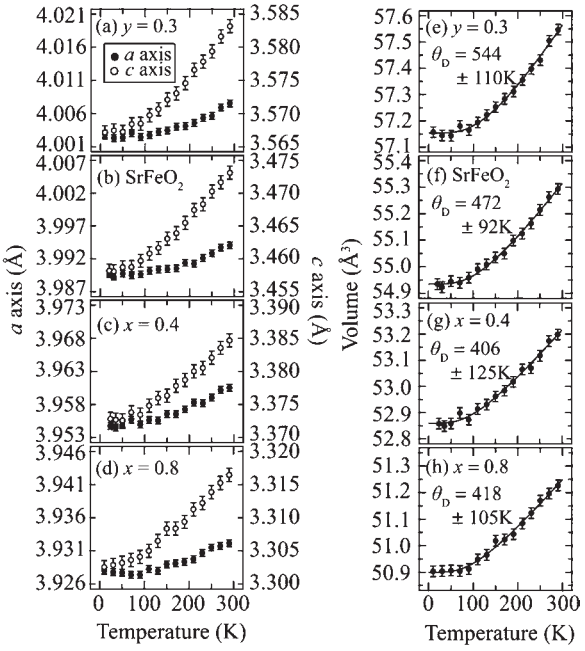

Figure 8. Lattice parameters and unit-cell volumes of $(Sr_{1-x}Ca_x)FeO_2$ and $(Sr_{1-y}Ba_y)FeO_2$ at low temperature. (a)−(d) Closed and open circles represent the a and c axes, respectively. (e)−(h) Circles represent the unit-cell volumes of $(Sr_{1-x}Ca_x)FeO_2$ and $(Sr_{1-y}Ba_y)FeO_2$ and solid lines represent the fit to the Debye−Grüneisen model with θ_D as an adjustable parameter. The present result of $SrFeO_2$ is in agreement with the result from a previous study (θ_D = 395 K)[11] calculated from the low-temperature XRD measurement without calibrations by Si.

between the theory and the experiment calls for further theoretical investigations. Here, the *IS* values for y = 0.1, 0.2, 0.3 that scarcely alter from that for $SrFeO_2$ might give us a hint. Since *IS* provides information on how strongly Fe atom is bonded, the observation implies that the reduced J_1 and J_2 (with y) must be compensated by the increase of other further-neighbor exchange integrals.

3.3. Thermal Stability. Low-temperature XRD measurements for x = 0, 0.4, 0.8 and y = 0.3 revealed the absence of any structural instabilities at low temperatures (Figure S5−S8). For the quantitative estimation of the lattice stiffness,[20−22] we calculated the Debye temperature θ_D

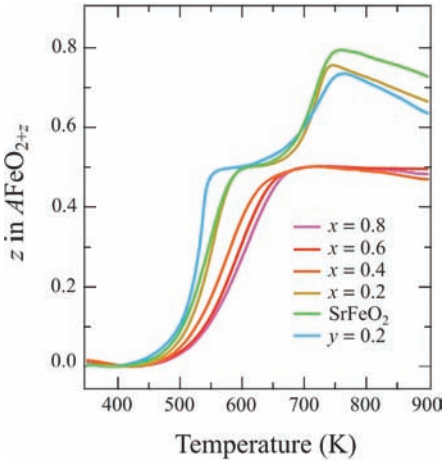

Figure 9. TG measurements of $(Sr_{1-x}Ca_x)FeO_2$ and $(Sr_{1-y}Ba_y)FeO_2$ performed in air. We normalized the raw TG data such that the plateaus correspond to the brownmillerite phase. It is to be noted that there is no intermediate phase for $0 < z < 0.5$ and hence the specimen in this z range is nothing but $(1-2z)$:$2z$ mixture of $AFeO_2$ and $AFeO_{2.5}$ phases.

using the Debye−Grüneisen model for the variation of unit-cell volume (see Figure 8), which is expressed as,

$$V(T) \cong V(0) + \int_0^T \frac{\gamma C_v}{B}\,dT \cong V(0) + \frac{9\gamma N k_B}{B} T\left(\frac{T}{\theta_D}\right)\int_0^{\theta_D/T} \frac{x^3}{e^x - 1}\,dx \qquad (1)$$

where $V(0)$ is the unit-cell volume at 0 K, γ is the Grüneisen parameter, B is the bulk modulus, k_B is the Boltzmann constant, and N is the number of atoms in the unit cell.[23,24] It is seen that the obtained values of θ_D are independent of composition within the experimental uncertainty, and are much smaller than that of $CaFeO_2$ with the distorted IL structure (θ_D = 733 K).[11]

The stability and reactivity of the IL structure at high temperature was investigated by the TG measurements in air up to 900 K (Figure 9). Compounds with a smaller r_A (x = 0.4, 0.6, 0.8) exhibited a single-step absorption of oxygen, while those with a larger r_A (x = 0.2, 0.0 and y = 0.2) did a double-step absorption with a single plateau. Since the starting materials contain a tiny yet finite amount of amorphous impurity phase as revealed by the Mössbauer study, a direct determination of the oxygen content for the target compound from the raw data was not possible. Nevertheless, sample identification was carefully made by ex-situ XRD after rapid quenching of the furnace at any point of the TG curve, and we found that the plateau corresponds to the $AFeO_{2.5}$ phase, and this phase for x = 0.2, 0.0 and y = 0.2 is further oxidized to become the pseudocubic oxygen-deficient perovskite. There is no intermediate phase between $AFeO_2$ and $AFeO_{2.5}$, as already pointed out for $SrFeO_2$.[4] With this knowledge, we normalized the raw TG data such that the oxygen content in the plateau region is 2.5 as shown in Figure 9.

(20) Okuda, T.; Asamitsu, A.; Tomioka, Y.; Kimura, T.; Taguchi, Y.; Tokura, Y. *Phys. Rev. Lett.* **1998**, *81*, 3203–3206.
(21) Ghivelder, L.; Castillo, I. A.; Gusmão, M. A.; Alonso, J. A.; Cohen, L. F. *Phys. Rev. B* **1999**, *60*, 12184–12190.
(22) Tohei, T.; Kuwabara, A.; Oba, F.; Tanaka, I. *Phys. Rev. B* **2006**, *73*, 64304.
(23) Kiyama, T.; Yoshimura, K.; Kosuge, K. *Phys. Rev. B* **1996**, *54*, R756–759.
(24) Dabrowski, B.; Avdeev, M.; Chmaissem, O.; Kolesnik, S.; Klamut, P. W.; Maxwell, M.; Jorgensen, J. D. *Phys. Rev. B* **2005**, *71*, 104411.

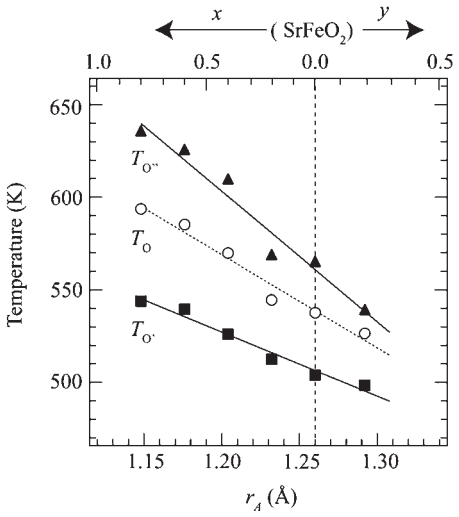

Figure 10. r_A dependence of T_O, $T_{O'}$ and $T_{O''}$, the temperatures at which the TG curves cross $z = 0.25$, 0.1, and 0.4 in Figure 9, respectively. Solid lines were obtained by a least-squares fit. We would like to note that there exists no intermediate phase between $z = 0$ and 0.5 in $A\mathrm{FeO}_{2+z}$.

Notably, the oxygen-absorbing temperature on forming $A\mathrm{FeO}_{2.5}$ systematically changes with chemical substitution. We define here T_O, $T_{O'}$, and $T_{O''}$ as a temperature at which the normalized TG curve crosses $z = 0.25$, 0.1, and 0.4, respectively, and are depicted as a function of r_A in Figure 10. T_O drops from 594 K for $(\mathrm{Sr}_{0.2}\mathrm{Ca}_{0.8})\mathrm{FeO}_2$ to 527 K for $(\mathrm{Sr}_{0.8}\mathrm{Ba}_{0.2})\mathrm{FeO}_2$. Obviously, T_O decreases in proportion with r_A. However, this would not mean that the IL structure becomes destabilized with increasing r_A because θ_D of the IL compounds is independent of the substitution (except the distorted IL structure CaFeO_2) and also because $(\mathrm{Sr}_{0.2}\mathrm{Ca}_{0.8})\mathrm{FeO}_2$ ($x = 0.8$) with the most deviated valences of A and Fe has the highest T_O. It is most probable that the dominant factor for controlling oxygen absorption behavior is the lattice parameters controlled by A-site cation size. Considering the facts that the c axis is more susceptible to r_A than the a axis and the oxygen pathways for the insertion of oxygen atoms may mainly involve the interlayer space between FeO_2 layers, we believe the c parameter contributes more to the oxygen absorbing temperature. However, one should recall that the conversion from the IL structure SrFeO_2 to the brownmillerite structure $\mathrm{SrFeO}_{2.5}$ involves not only the insertion of oxygen atoms but also the reconstruction of the Fe−O framework.[4] Recent thin film studies have shown two distinct reaction pathways with different kinetic energies.[25] Furthermore, the slope for the $A\mathrm{FeO}_2$ to $A\mathrm{FeO}_{2.5}$ conversion becomes steeper with r_A; the difference between $T_{O''}$ and $T_{O'}$ is about 100 K for $(\mathrm{Sr}_{0.2}\mathrm{Ca}_{0.8})\mathrm{FeO}_2$, while about 50 K for $(\mathrm{Sr}_{0.8}\mathrm{Ba}_{0.2})\mathrm{FeO}_2$. Thus it might be possible that the oxygen migration pathways are also influenced by r_A.

4. Conclusion

We demonstrated that SrFeO_2 with the IL structure can tolerate only up to 30% substitution of Ba unlike the case of Ca-substitution. The long Fe−O distance caused by the Ba-substitution destabilizes the IL structure. The negative pressure effect does not drastically change the magnetic properties in contrast to the theoretical anticipation, meaning that iron atoms are still very strongly bonded to oxide ion. The oxidation temperature and rate are controllable to a great extent by A-site cation size. The importance of interstitial oxide ions has been recently stressed for the design of oxygen ion conductors.[26−28] In the present compounds, no phase could be found between $A\mathrm{FeO}_2$ and $A\mathrm{FeO}_{2.5}$ although more oxidized phase $\mathrm{SrFeO}_{3-\delta}$ ($0 < \delta < 0.5$) are known to exhibit high oxide ion conductivity. But, the elongated c-axis with respect to SrFeO_2 may allow further manipulation of structures, for example, by oxidative intercalation by chlorine gas.

Acknowledgment. We thank Myung-Hwan Whangbo for a helpful advice about magnetism, Yoshihiro Tsujimoto and Takashi Watanabe for helpful discussions, Kenichi Kato and Kim Jungeun for the support of the synchrotron X-ray diffraction experiments, Kenji Nemoto for the support of the neutron powder diffraction experiments, Kazuyoshi Kanamori for the support of the thermogravimetric measurements. This work was supported by Grants-in-Aid for Science Research (No. 19052004 and No.22245009) from the Ministry of Education, Culture, Sports, Science and Technology of Japan, and by the Global COE program International Center Science, Kyoto University, Japan.

Supporting Information Available: Experimental details and characterization data for the new compounds. This material is available free of charge via the Internet at http://pubs.acs.org.

(25) Inoue, S.; Kawai, M.; Ichikawa, N.; Kageyama, H.; Paulus, W.; Shimakawa, Y. *Nat. Chem.* **2010**, *2*, 213–217.

(26) Demourgues, A.; Wattiaux, A.; Grenier, J. C.; Pouchard, M.; Soubeyroux, J. L.; Dance, J. M.; Hagenmuller, P. *J. Solid State Chem.* **1993**, *105*, 458–468.

(27) Boehm, E.; Bassat, J. M.; Steil, M. C.; Dordor, P.; Mauvy, F.; Grenier, J. C. *J. Solid State Sci.* **2003**, *5*, 973–981.

(28) Kuang, X.; Grean, M. A.; Niu, H.; Zajdel, P.; Dickinson, C.; Claridge, J. B.; Jantsky, L.; Rosseibsky, M. J. *Nat. Mater.* **2008**, *7*, 498–504.